RSC Advances

ROYAL SOCIETY OF CHEMISTRY

www.rsc.org/advances

RSC Advances

ARTICLE

Design and Fabrication of Hollow and Filled Graphene-based Polymeric Spheres via Core-Shell Electrospraying

Received 00th January 20xx,
Accepted 00th January 20xx

DOI: 10.1039/x0xx00000x

www.rsc.org/

Leila Haghighi Poudeh[a], Burcu Saner Okan[b,*], Jamal Seyyed Monfared Zanjani[a], Mehmet Yildiz[a], Yusuf Menceloglu[a]

Two dimensional graphene oxide sheets are converted into three dimensional (3D) hollow and filled microspheres by using three different carrying polymers through one-step core-shell electrospraying technique without applying any post treatments. Electrospraying process prevents the aggregations and crumbling of graphene sheets by constructing 3D interconnected framework, and provides homogeneous dispersion of graphene sheets in polymer solution under electric field, and allows the polymer chains to crawl into graphene layers forming intercalated structure. The proper polymer concentration and solution viscosity are determined by using Mark-Houwink-Sakurada equation to produce an ideal graphene based polymeric sphere structure via electrospraying. Graphene based polymeric spheres with controllable hollowness are successfully fabricated by changing core solvents. The connectivity of graphene sheets in polymeric shell is improved by increasing carbon networks after carbonization process. Morphology, shrinkage behaviour and structural properties of spheres are evaluated by tailoring polymer type, polymer concentration, graphene amount, flow rate and applied voltage.

Introduction

Graphene with a 2D honeycomb-like structure of carbon atoms has been used in many applications including microchips, sensors, energy storage devices, and composites due to its unique mechanical, thermal and electronic properties[1]. There are two main approaches in the synthesis of 2D graphene; bottom-up approach consisting of epitaxial growth on silicon carbide and chemical vapor deposition (CVD) method, and top-down approach including micromechanical cleavage, electrochemical exfoliation and chemical exfoliation of graphite. The advantage of using bottom-up approach is controlling the morphology and structure of the produced graphene sheets[2], whereas top-down methods have some drawbacks of preserving 2D structure of graphene and limitations in the utilization of graphene in polymer matrix and transferring graphene sheets on different templates[3]. Graphene sheets have tendency to agglomerate in matrix and form crumpled structure which causes a significant decrease in the surface area, electrical and other characteristic properties[4]. To overcome this problem, several studies have focused on the development of 3D graphene materials with different structures and morphologies such as graphene fibers[5,6], graphene tubes[7], graphene balls[8] and, graphene networks[9,10]. CVD technique is one of the widely used bottom-up approaches for the production of 3D graphene networks, 3D porous graphene films and macroporous structures over templates such as conductive substrates and 3D metal substrates (e.g. nickel foam) by using different carbon sources at different conditions[11–13]. It is also possible to convert 2D graphene sheets into 3D structures by wet chemistry methods like water-in-oil emulsion technique without using any surfactant[14] and hydrothermal process by mixing graphene oxide (GO) with carbon nanotubes and metal oxides to improve surface area, electrical conductivity and capacitance properties of 3D graphene structures[15,16]. In the recent works, thermoelectric properties of graphene based nanocomposites have been improved by constructing 3D interconnected structures consisting different conducting polymers and reduced graphene oxide (rGO) by *in situ* polymerization techniques[17–19]. Especially in flexible energy storage devices, graphene based fibers and 3D porous graphene polymer networks are fabricated as an electrode material in supercapacitors to enhance specific capacitance and provide long-term cyclic stability[20,21].

For the production of hollow 3D graphene structures, sphere-like templates such as polystyrene (PS), silicon dioxide (SiO_2), and titanium dioxide (TiO_2) were used in several published techniques. In one of the works, graphene hollow spheres were prepared by covering PS balls with graphene oxide (GO) sheets and then

[a] Faculty of Engineering and Natural Sciences, Sabanci University, Tuzla, Istanbul 34956, Turkey,Email: meyildiz@sabanciuniv.edu
[b] Sabanci University Nanotechnology Research and Application Center, SUNUM, Tuzla, Istanbul 34956, Turkey

calcination was applied at 420˚C for 2h to remove PS from the core[22]. In another work, graphene-based hollow spheres were fabricated by electrostatic assembly of GO sheets on polyethylenimine covered SiO_2 spheres in solution phase, and subsequently followed by washing with hydrofluoric acid and annealing processes to get hollow structure[23]. In order to improve the catalytic properties of hollow spheres, Pd nanoparticles were decorated in double-shelled hollow carbon spheres by using SiO_2 nanospheres as template during *in situ* process[24]. In the mentioned processes, the size of spheres directly depends on the templates. It is not an easy process to control the shape of spheres and hollowness and get higher yield of graphene balls due to the recovery process in wet-chemical methods.

Electrospinning is one of widely used techniques to produce fibers and spherical or bead-like structures with the diameters ranging from few micrometers to nanometer by adjusting the surface tension of the droplet and viscosity of the solution under electric field[25]. Recently, co-axial electrospinning process has received great attention due to its ability to produce core-shell 3D structures with different functionalities which have distinct advantages in comparison to structures fabricated by regular electrospinning technique[26]. In this technique, two dissimilar solutions in concentric tubes flow under a high electric field, which is applied between the tip of the nozzle and collector. As a result, the surface tension of a compound droplet at the tip of the nozzle is overcome whereby the droplet stretches and forms a continuous jet which is collected on the electrically grounded plate as a fiber[27]. In electrospinning and electrospraying, the final morphology of the product is affected by solution properties (such as viscosity and electrical conductivity) and process parameters (such as voltage, flow rate, and distance between collector and nozzle). There are few attempts for the integration of graphene into the fiber structure by using classic and co-axial electrospinning techniques. In one of the studies, Promphet et al.[28] fabricated graphene based nanoporous fibers by electrospinning of graphene/polyaniline/polystyrene mixture to be used as an electrochemical sensor to detect heavy metals. In another work, aligned poly(3-hexylthiophene)–graphene nanofibers produced via two-fluid coaxial electrospinning technique were integrated into high-performance field effect transistors since graphene acts as an electronically conducting bridge between the polymer domains in the structure[29]. Shilpa et al.[30] synthesized core-shell composite nanofibers as an anode electrode for Li-ion batteries by co-axial electrospinning of rGO-polyacrylonitrile (PAN) solution as shell and zinc oxide with polymethyl methacrylate (PMMA) as core and then applied carbonization and calcination processes to this fiber mat. In all above mentioned relevant studies, for preserving the intrinsic properties of graphene materials in the bulk matrix, GO and rGO are incorporated into the fiber structure by electrospinning technique in one-step process.

One can conclude from literature that so far, considerable amount of works have focused on the production of polymeric bead structures and core-shell microcapsules and the investigation of their morphological changes by tailoring electrospinning parameters[31,32]. In the present work, thermally exfoliated graphene oxide (TEGO) sheets are converted into 3D spheres with controlled hollowness and porosity by using three different carrier polymers through core-shell electrospraying technique. The effect of electric field on the exfoliation of graphene sheets is investigated by spectroscopic techniques to understand graphene dispersion behavior in polymeric shell during electrospraying process. In this study, shell polymers namely PS and PMMA are chosen due to their ease for the formation of spherical topology during electrospinning process since these two polymers are widely used as a template material for the production of 3D structures. Additionally, PAN polymer is used to form carbon network because of its high carbonization degree. The appropriate concentration for the production of spheres is verified by using Mark-Houwink-Sakurada equation. Hollowness of these spheres is controlled by changing core solvent and its flow rate. The dimension and morphology of graphene based spheres are investigated and optimized by tailoring the parameters of polymer type, polymer concentration, solution viscosity, TEGO amount, solvent evaporation rate and flow rate.

Experimental

Materials

The following materials were used in the experiments: TEGO-grade 2 (Thermally exfoliated graphene oxide purchased from NANOGRAFEN Co., average number of graphene layers: 27 calculated from X-ray diffraction data, 4% oxygen content obtained from X-ray photoelectron spectroscopy), N, N-dimethyl formamide (DMF, Sigma Aldrich, 99%), and methanol (Sigma Aldrich, 99.7%). Polystyrene (PS), Polymethyl Methacrylate (PMMA) and Polyacrylonitrile (PAN) were synthesized through free radical polymerization method. A detailed synthesis procedure of PS and PMMA polymers and their characterization results were reported in our previous publication[33].

Preparation of electrospraying solutions

TEGO-based polymeric solutions were prepared as shell materials. PS and PMMA solutions were prepared with a concentration of 20 wt% in DMF solvent. For PAN polymer, 5 wt% and 3.5 wt% were selected as polymer concentration due to its high viscosity. TEGO was dispersed in DMF at different TEGO:DMF weight ratios of 0.005, 0.01, 0.02, and 0.05 % by probe sonicator (Qsonica, Q700) for 20 minutes with 5 seconds pulse on and 3 seconds pulse off time in ice bath to get homogeneous dispersions in solutions. Then, polymers were added into TEGO dispersed DMF solution and the mixtures were stirred at room temperature for 1 day to improve the stabilization of polymer chains. The chemical structures of synthesized polymers are given in **Fig. S1** (refer to supplementary document).

Production of TEGO based 3D hollow and filled polymeric spheres by core-shell electrospraying

Core-shell electrospraying process was performed by following two different procedures. In the former one, the

core was kept empty during spraying process and atmospheric air was used as a core material. In the latter one, methanol was used as a core solvent to study the effect of methanol on the hollowness and morphology of spheres. Three different polymeric solutions with different TEGO contents were used as shell materials. **Fig. 1** shows schematic representation of graphene based sphere fabrication by tri-axial core-shell electrospraying technique. The size of spheres was controlled by solution parameters (type of polymer, viscosity, surface tension, concentration, and evaporation rate of solvent) and system parameters (voltage, distance between collector and syringe, flow rate) through electrospraying process. Electrospraying is performed at ambient conditions by using tri-axial electrospinning equipment purchased from Yflow Company. All the spheres were sprayed with a nozzle to collector distance of 10 cm to study the effect of applied voltage and flow rate on the size of the spheres. The applied voltage was in the range of 10–20 kV. The flow rates of shell solutions varied between 10-20 µL/min. Methanol as a core solvent was sprayed with a flow rate in the range of 0.5-2 µL/min. Electrospraying parameters of the produced spheres are given in details in **Table S1**.

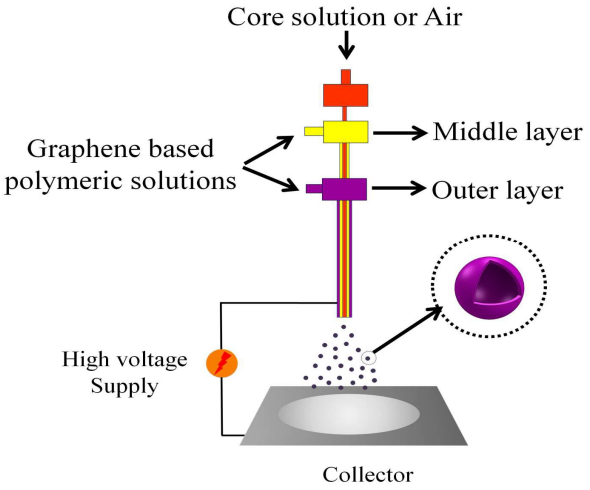

Fig. 1 Schematic representation of fabrication of graphene based spheres by tri-axial electrospraying technique.

Carbonization process of produced spheres

Carbonization of TEGO based PAN spheres was completed in two steps. Firstly, spheres were stabilized by an oxidation process by heating up to 300°C under air, and then carbonization step was followed by increasing the temperature up to 1000°C under argon atmosphere. Stabilization process changes the chemical structure of spheres and the produced spheres become thermally stable at higher temperature without transition to melting phase[34].

Characterization

Molecular weights and polydispersity index of polymers are measured in DMF as an eluent by using Gel Permeation Chromatography (GPC) and also the concentrations of polymers in column are converted to the intrinsic viscosity. The morphology and inside structure of spheres were analyzed by Leo Supra 35VP Field Emission Scanning Electron Microscope (SEM) and JEOL JIB 4601F Focused Ion Beam (FIB/SEM dual beam platform). Elemental analysis of spheres was conducted by using Energy-Dispersive X-Ray (EDX) analyzing system. X-ray diffraction (XRD) measurements were carried out by using a Bruker AXS advance powder diffractometer with a CuKα radiation source. Raman spectroscopy was used to identify the surface characteristics of samples by using a Renishaw inVia Reflex Raman Microscopy System with the laser wavelength of 532 nm at room temperature in the range of 100–3500 cm^{-1}. The functional groups of spheres were determined by Netzsch Fourier Transform Infrared Spectroscopy (FTIR).

Results and Discussion

The effect of electric field on the exfoliation process of TEGO sheets

Electrospraying process enables graphene sheets to get dispersed homogeneously in polymer solution, prevents their agglomeration under electric field and enhances the intercalation of polymer chains into graphene layers. SEM images of TEGO sheets after the sonication and electrospraying processes are given in **Fig. 2** to promote understanding the effect of electric field on the morphological changes of TEGO sheets. Untreated TEGO has worm-like structure (**Fig. 2a**). After sonication in DMF, layers are separated from each other, and hence, flake dimension decreases (**Fig. 2b**); however, the structure still has multi-layered graphene[35]. Upon the being subjected to applied electric field, the layers become more flattened whereby more transparent sheet formation is observed (**Fig. 2c**). Electric field deforms the working fluid during electrospraying which causes loosely broad graphene layers.

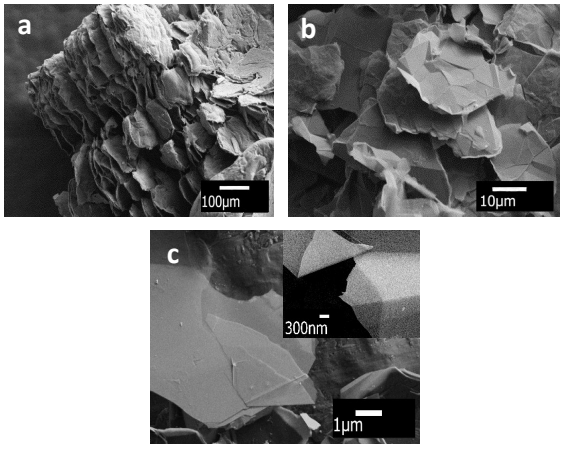

Fig. 2 SEM images of (a) as received TEGO sheets, (b) sonicated TEGO sheets in DMF, and (c) electrosprayed TEGO sheets in DMF without polymer.

In order to detect the changes in the number of graphene layers, Raman Spectroscopy analysis was conducted for as received, sonicated and electrosprayed TEGO sheets and the results are presented in **Fig. 3**. Raman spectrum of TEGO has three sharp main peaks: 1338 cm^{-1}, 1577 cm^{-1}, and 2750 cm^{-1}, refer to as D, G, and 2D peaks, respectively[36]. D peak is related to disorderness and its intensity changes with the defects in the structure. G peak corresponds to in-plane vibrations of sp^2 bonded carbon atoms and its intensity is altered due to the variation in the number of graphene layers[36,37]. It is known from literature, as the ratio of D to G intensities (I_D/I_G) increases, sp^2 bonds are broken implying that there are more sp^3 bonds and more defects in the structure[36]. In the current study, after the sonication process, there is a slight decrease in I_D/I_G of untreated TEGO sample from 0.2 to 0.1. After eletrospraying of TEGO sheets, D band completely disappears indicating that defect-free multi-layer graphene sheets are obtained. This decrease in D band intensity comes from the reduction in the thickness of graphene layers which is due to the deformation of solvent. In addition, shape, width and position of 2D peak determine the graphene layers[36]. The reduction in the intensity ratio of G to 2D peaks (I_G/I_{2D}) indicates the decrease in the number of graphene layers. I_G/I_{2D} values of untreated TEGO and sonicated TEGO, and electrosprayed TEGO are 2.3, 2.0 and 2.0, respectively. This shows that the sonication process breaks down graphene layers, which are bonded by weak van der Waals forces, and then initiates the exfoliation process. On the other hand, multi-layer structure is still preserved after electrospraying process because there is no notable change in I_G/I_{2D} value. Furthermore, the intensity values of 2D peak increases after each process, and 2D peak of electrosprayed TEGO gets sharper and thus number of graphene layers decreases slightly when compared to sonicated TEGO. The peak positions and intensity ratios are given in **Table S2.**

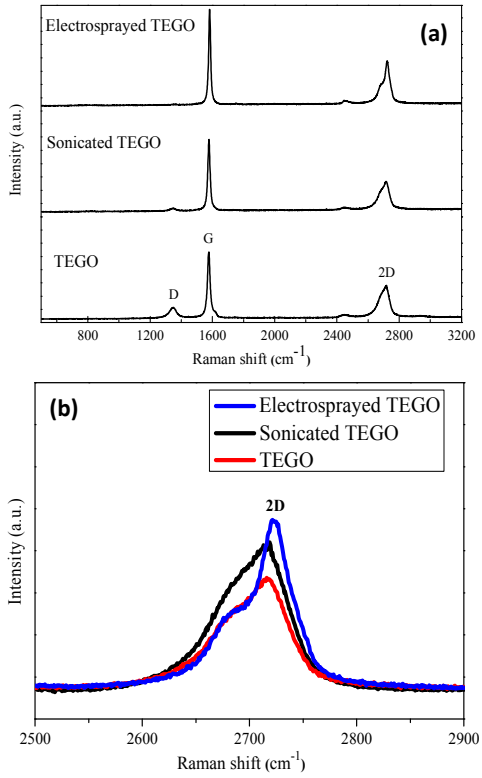

Fig. 3 (a) Raman spectra of as received TEGO, sonicated TEGO and electrosprayed TEGO and (b) the comparison of 2D peak intensities.

The effect of polymer type, polymer concentration and TEGO amount on the structural properties of graphene-based spheres.

In the electrospraying process, the viscosity of solution is one of the important parameters, which determines the morphology of structure. The higher the viscosity is, the greater the electric field should be to be able to deform the droplet at the nozzle tip to initiate the polymeric jet formation. The viscosity of solution depends on the molecular weight of polymer and polymer concentration. PS, PMMA, and PAN as thermoplastic polymers are chosen as shell materials in the production of polymer-based composites via core-shell electrospraying process. Weight average molecular weight (Mw), number average molecular weight (Mn), polydispersity index (PDI) and intrinsic viscosity values of the used polymers are given in **Table 1**. These polymers have similar Mw values but their intrinsic viscosity values are different and this directly affects polymer concentration and viscosity of electrospun solutions.

Table 1: Mw, Mn, PDI and intrinsic viscosity values of shell polymers from GPC analysis

Polymer type	Mw (g/mol)	Mn (g/mol)	PDI	Intrinsic viscosity (dL/g)
PMMA	41645	20798	2.00	0.3404
PS	49283	29686	1.66	0.0781
PAN	44489	32293	1.38	0.7261

Selected polymers can form spherical structures by the optimization of the system (applied voltage, syringe and collector distance, flow rate) and solution parameters (polymer concentration and TEGO content). In addition to these mentioned parameters, polymer chain entanglements affect the structural formations during electrospinning process. The degree of entanglement is determined by calculating two limiting concentrations, C* and C_e. C* corresponds to the solution concentration where the hydrodynamic volumes begin to overlap and C_e is the entanglement concentration which separates the semi-dilute unentangled and semi-dilute entangled regimes. C* is calculated using the following equation:

$$C^*=1/[\eta] \quad (1)$$

where [η] is the intrinsic viscosity[31]. C_e value is approximately equal to 10C* for neutral polymers in good solvent systems[38]. When polymer concentration, C, is higher than C_e, bead free fibrous structures are produced due to the extensive chain entanglement. When $C^*<C<C_e$, bead dominant structures are generated[31]. In this study, C* values of PMMA and PS are about 29.4 mg/mL and 128.1 mg/mL, respectively and the adjusted concentrations (C) of PMMA and PS are 200 mg/mL which is in the range of $C^*<C<C_e$. In case of PAN based spheres, C* is about 13.8 mg/mL and polymer concentrations of 3.5 wt% and 5 wt% are 35 mg/mL and 50 mg/mL, respectively, and these values are between C* and C_e.
Moreover, the optimum concentration for the fabrication of polymer based TEGO spheres was investigated by using Mark-Houwink-Sakurada equation (Eq.2):

$$[\eta]=K_H M^a \quad (2)$$

where the constants "K_H" and "a" depend on the polymer type, solvent and temperature. The Mark-Houwink-Sakurada constants of PMMA, PS, and PAN are given in **Table S3**. By combining Eq.1 and Eq.2, following expressions based on C* and molecular weight is obtained for each polymer:

$$C^*= 4\times10^{4}Mw^{-0.625} \quad \text{PMMA} \quad (3)$$

$$C^*= 3.15\times10^{4}Mw^{-0.603} \quad \text{PS} \quad (4)$$

$$C^*= 5.65\times10^{4}Mw^{-0.780} \quad \text{PAN} \quad (5)$$

Fig. 4 shows the entanglement concentration C_e=10C* as a function of molecular weight of PMMA, PS, and PAN polymers. Solid lines represent the concentration threshold of each polymer obtained from Eq.3 (black line), Eq.4 (red line) and Eq.5 (blue line), and each point corresponds to the polymer concentrations which are selected for the fabrication of spheres. As seen in **Fig. 4**, all of the corresponding points attributed to the used polymer concentrations stay on the lower region of threshold line (C_e) where bead formation is dominant.

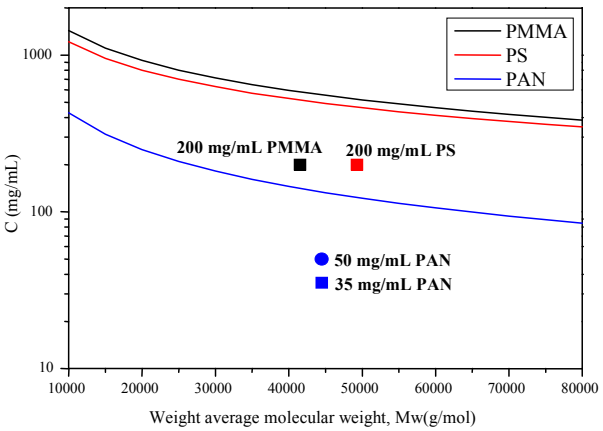

Fig. 4 Entanglement concentration Ce=10C* as a function of the molecular weight of PMMA, PS, and PAN polymers.

Polymeric solutions were purged through outer syringe by keeping core syringe empty during co-axial electrospraying. Table 2 summarizes the synthesis conditions and characteristic properties of spheres made of PMMA and PS polymers and shrinkage percentages of polymeric spheres after the integration of TEGO into the structure. By the addition of TEGO in electrospun solutions, there is a significant decrease in the diameter of TEGO based spheres when compared to neat polymeric spheres. Herein, TEGO sheets start the shrinkage of the spheres under electric field since the surface forces increase on droplets. After increasing the amount of TEGO, a gradual increase is observed in sphere diameter. For instance, as seen in Table 2, PMMA spheres shrink by about 38% through the addition of 0.005 wt% TEGO and the shrinkage values decreases down to 29% and 20% with 0.01 wt% and 0.02 wt% TEGO loadings, respectively. The decrease in diameter shows the dense stacking of graphene layers in polymeric shell. It is known that oxygen functional groups of GO in aqueous and organic solutions are negatively charged[39], and hence, the electrostatic interaction between these negatively charged GO sheets and positively charged polymers minimizes the size of the spherical structure. Carbon/oxygen ratio of GO is changed regarding the type of chemical exfoliation process[35,40]. Most of surface oxygen functional groups can be removed by applying thermal treatment and hydrophilicity of GO decreases and this allows for controlling the surface chemistry of graphene[41]. In addition, thermal treatment extends the distance between graphene layers and ease intercalation process is achieved during electrospraying process. Therefore, TEGO is preferred as filler for the production of composite spheres. Increasing TEGO amount in electrospun solution gradually imbalances the electrostatic interaction between charges, and enlarges the sphere diameter.

Table 2: Synthesis conditions and characteristics of TEGO based PMMA and PS spheres and their shrinkage percentages.

	TEGO amount (wt%)	Average diameter of spheres (µm)	Average shrinkage of spheres (%)
PMMA	0	4.7	-
	0.005	2.9	38
	0.01	3.4	29
	0.02	3.8	20
PS	0	4.5	-
	0.005	2.2	51
	0.01	2.6	42
	0.02	3.1	32

Fig. 5 exhibits SEM images of spheres sprayed by using air at atmospheric pressure in the core of the syringe. After electrospraying process without any core materials, it is observed that all types of polymers form porous and filled sphere structures. After the addition of TEGO into the polymer, it is noted that the diameter of these spheres decreases. Furthermore, **Fig. 6** presents SEM images of neat PS spheres and TEGO based PS spheres at higher magnification. By the incorporation of TEGO, the porosity of spheres decreases and the surface becomes smoother.

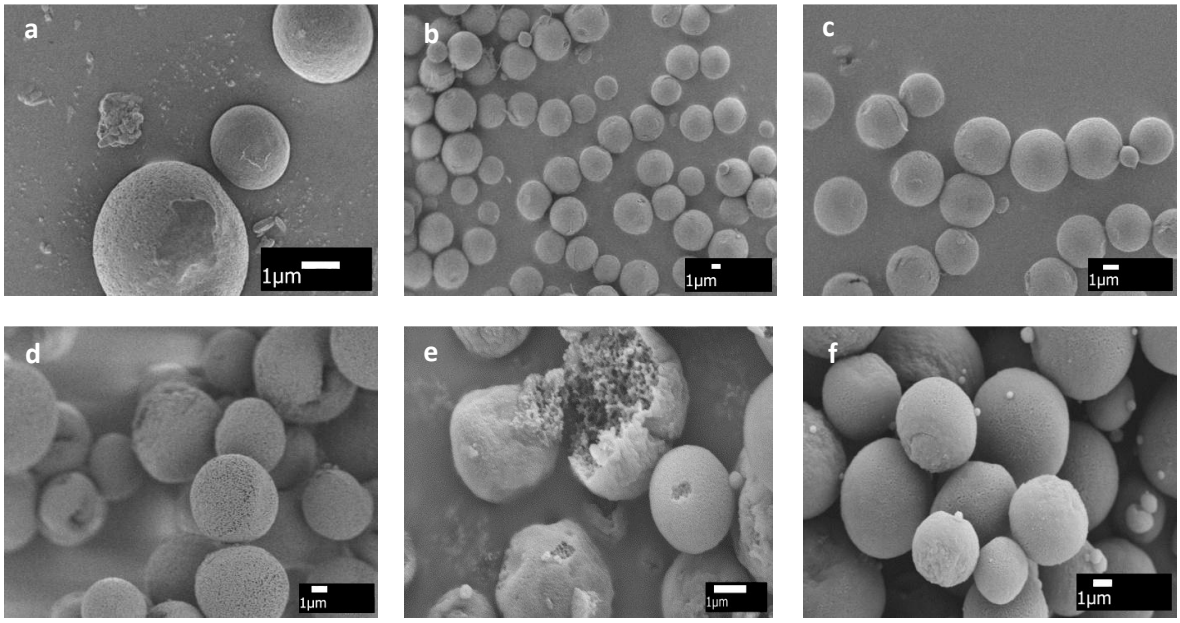

Fig. 5 SEM images of spheres produced by (a) PMMA, (b) PMMA-0.01 wt% TEGO, (c) PMMA-0.02 wt% TEGO, and (d) PS, (e) PS-0.005 wt% TEGO, (f) PS-0.02 wt% TEGO.

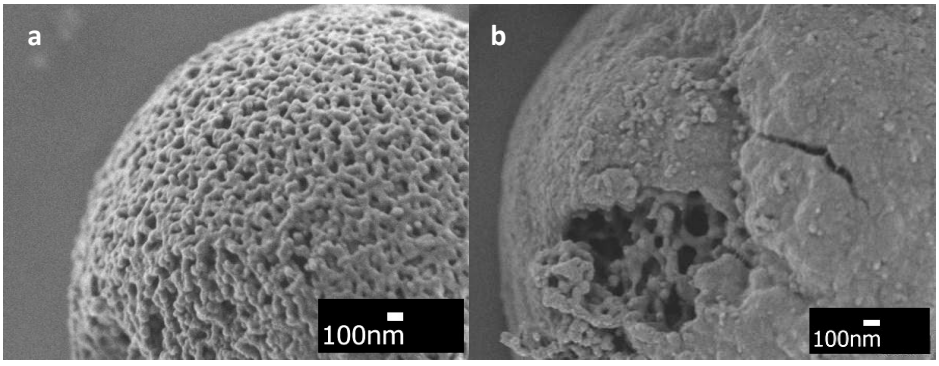

Fig. 6 SEM images at higher magnifications of (a) PS spheres and (b) PS-0.005 wt% TEGO spheres.

RSC Advances

ARTICLE

XRD characterization was performed in order to prove the presence of TEGO in polymer spheres. In **Fig. 7**, TEGO has a characteristic 002 peak at 26.5°. In the XRD analysis of polymer-graphene based nanocomposites, 002 peak can either completely disappear or shift to the lower region due to the intercalation of polymeric chains into graphene sheets[42,43]. In **Fig. 7a**, PMMA shows a wide diffraction peak spanning from 10˚ to 20˚ with a maximum intensity at 2Θ≈14.4˚ and the intensity of this peak decreases as TEGO amount increases and 2Θ shifts to lower angel values due to the complete coating of multi layer graphene by polymer chains. Also, the diffraction peak broadens and its intensity decreases by the incorporation of TEGO and thus composite becomes completely amorphous structure. In **Fig. 7b**, PS has a broad diffraction peak between 15˚ and 25˚ and as the value of TEGO increases, PS diffraction peak shifts towards lower angles and its peak becomes wider by increasing TEGO amount. **Table S4** of supplementary document also shows the values of polymer peak intensity and 2Θ values. One can note that in the produced spheres, 002 peak of TEGO disappears. The slight shifting of polymer diffraction peak to the lower angle region and the disappearance of 002 peak of TEGO bespeak that the electric field enhances the distribution of graphene sheets in polymer solution so that multi-layer graphene sheets are completely coated by polymer during sphere formation. **Fig. 8** also shows schematically how complete coverage occurs between TEGO and polymer chains and avoids restacking of multi-layer graphene sheets under electric field.

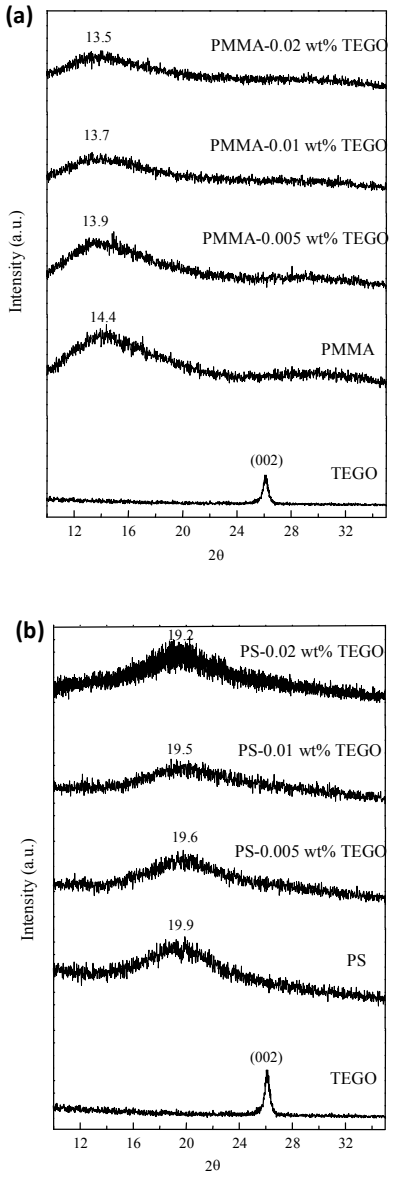

Fig. 7 XRD spectra of (a) PMMA-TEGO spheres and (b) PS-TEGO spheres.

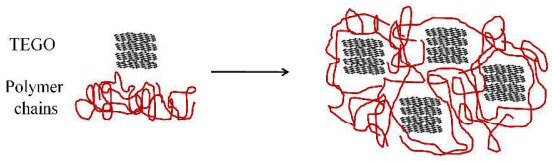

Fig. 8 Schematic illustration of interactions between polymeric chains and TEGO sheets during sphere formation.

Fig. 9 shows Raman spectra of TEGO, PS, and PS-TEGO spheres. PS has characteristic Raman peaks at 3050 cm^{-1} and 2900 cm^{-1} due to the vibration of C-H bonds, 1600 cm^{-1} attributed to C=C vibrations and 995 cm^{-1} related to aromatic carbon rings[44]. In the Raman spectrum of the PS-0.02 wt% TEGO, the characteristic peaks of TEGO do not appear because of the low amount of TEGO in the polymeric spheres and overlapping of polymer main peaks with TEGO peaks. On the other hand, significant decrease in Raman peaks of PS was observed by the integration of TEGO (see **Table S5** in supplementary document) which also proves the presence of TEGO in the spheres.

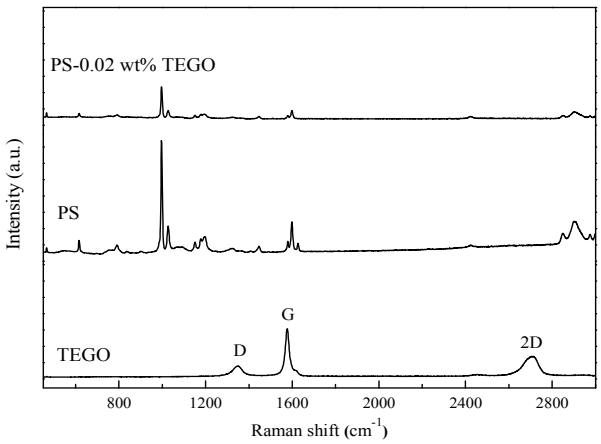

Fig. 9 Raman spectra of TEGO, PS spheres, and PS-0.02 wt% TEGO spheres.

The effect of core material on the hollowness of TEGO based polymeric spheres

In order to observe the effect of the core material on the hollowness of PMMA-TEGO spheres, methanol was used as a core solvent in electrospraying process. The shell solvent of polymer solution is DMF with a vapor pressure of about 516 Pa whereas methanol has higher vapor pressure about 13020 Pa. Shell formations and hollowness can be controlled by increasing solvent vapor pressure and tailoring flow rates. In addition, the evaporation rate depends on the flow rate of core solution so that three different flow rates are investigated to tailor the hollowness formation in the present study. Other system (voltage, distance between collector and syringe) and process (polymer concentration, type of solvent, TEGO amount) parameters were kept the same in each trial to see the effect of flow rate on the morphologies of spheres. As the evaporation rate of the core solvent increases, the solvent will have sufficient time for the evaporation. Hence, low flow rate of the core solution causes hollow sphere formation, the shell is formed initially and then core solvent evaporates through the pores of shell until the spheres reaches the collector. Surface forces have a significant role in shaping the surface of the jet and controlling the porosity[45]. As the flow rate of core solvent increases, the fast evaporation of core solvent causes local phase separation, and the solvent-rich regions leaves behind porous structures during the electrospraying process and thus porous and filled spheres are formed. Increasing the flow rate further (i.e., 5 µL/min) leads to fiber formation instead of spheres.

The produced spheres were cut by using an ion beam source of FIB-SEM instrument to investigate the inside of microstructures. **Fig. 10** displays FIB-SEM images of 0.02 wt% TEGO+PMMA spheres produced utilizing the methanol as core solvent with the lowest flow rate. Before the ion bombardment, spherical structure is clearly seen in 10a. After the ion bombardment, the shell material starts to melt upon increasing the current of the ion beam whereby one can clearly observe the hollowness within the sphere as seen in **Fig. 10b. Fig. 11** yields the FIB-SEM images of TEGO based PMMA spheres produced with a flow rate of 2 µL/min during the ion beam bombardment process. The porous core structure is detected at the end of complete melting of shell materials as seen in **Fig. 11c**. This proves that increasing the flow rate of core solvent facilitates the penetration of core solvent through shell and induces phase separations and thus leads to porous core structure. The average diameter of spheres changes from 3.4 µm to 4.6 µm by increasing the flow rate of core material because higher flow rate speeds up the evaporation process of solvent. Spraying methanol with a high flow rate of 5 µL/min totally changes the morphology and fiber formation is detected among spheres, which are shown in **Fig. S2**.

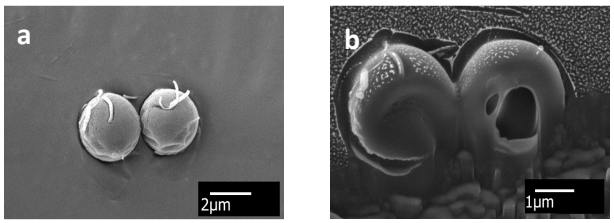

Fig. 10 FIB-SEM images of PMMA spheres containing 0.02 wt% TEGO using methanol as a core material and a flow rate of 0.5 µL/min (a) before and (b) after ion bombardment.

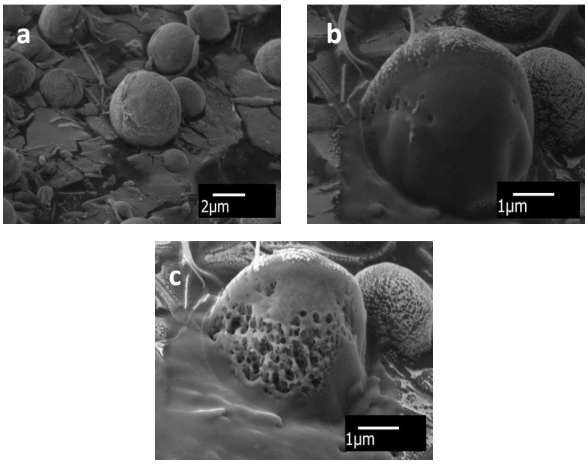

Fig. 11 FIB-SEM images of PMMA spheres containing 0.02 wt% TEGO using methanol as a core material and a flow rate of 2 µL/min (a) before and (b) during and (c) after ion bombardment.

In addition, FIB-SEM technique is used for the observation of porous core in PMMA spheres produced by using atmospheric air in core syringe. **Fig. 12** displays FIB-SEM images of these spheres after the ion bombardment. The structure of spheres is noticeably porous even at longer bombardment period.

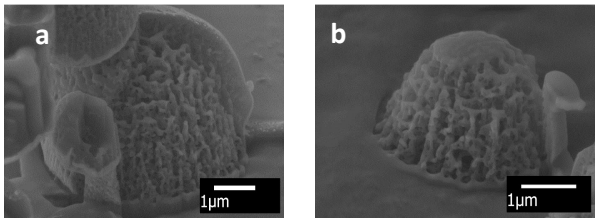

Fig. 12 FIB-SEM images of 20 wt% PMMA spheres containing 0.02 wt% TEGO by using atmospheric air as a core material (a) and (b) after ion bombardment.

The effect of carbonization on the morphology of TEGO based polymeric spheres

PAN polymer is one of the most important precursors of carbon source in the production of polymeric composites. Carbonization makes PAN polymer promising especially in energy applications because its electrical and mechanical properties are significantly improved by increasing carbon content up to 95%[34]. Instead of PS and PMMA used as template materials having lower degradation temperatures between 300-400°C, PAN is chosen as a carrying polymer for the carbonization process to form carbon network with graphene sheets since PAN undergoes heating process at high temperature in the range of 800-3000°C[34].

At the initial step of our process, 5 wt% PAN, 5 wt% PAN-0.02 wt% TEGO and 3.5 wt% PAN-0.05 wt% TEGO solutions were sprayed separately without using any core material to produce PAN-based spheres. Fabricated spheres containing 5 wt% PAN and 5 wt% PAN-0.02 wt% formed half hollow spheres (donut-shaped structures) and carbonization does not affect the morphologies of these structures as seen in **Fig. 13**. The reason for donut-shaped formation might be due to the combined effects of low polymer concentration, high intrinsic viscosity and applied electric forces. Thus, a rather interesting sphere structure is formed during the discharge process of the polymeric mixture from the tip of syringe. Average diameters of 5 wt% PAN and 5 wt% PAN-0.02 wt% TEGO spheres are about 1.6 μm and 2.9 μm, respectively. The incorporation of TEGO enlarges the diameter of spheres, which might stem from better dispersion and alignment of multi-layer graphene sheets in higher viscosity of PAN solution during electrospraying process when compared to the results of PMMA and PS solutions.

After the carbonization process, both neat PAN and TEGO based PAN spheres shrink about 75%, and the diameters of PAN and TEGO based PAN spheres decrease down to nanometer scale and become 400 and 700 nm, respectively. Carbonization leads to the formation of more packed spheres having less porosity (**Fig. 13b** and **13d**).

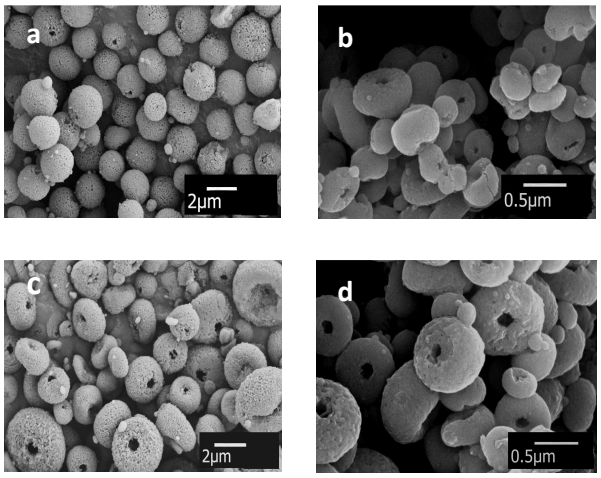

Fig. 13 SEM images of 5 wt% PAN spheres (a) before and (b) after carbonization, and 5 wt% PAN-0.02 wt% TEGO spheres (c) before and (d) after carbonization.

In another PAN sphere production, TEGO amount increased up to 0.05 wt% and polymer concentration decreased down to 3.5 wt% in order to investigate the changes in morphologies of spheres. By increasing TEGO content, the zero shear viscosity of electrospun solution is expected to increase which will require larger electric field strength to deform the droplet whereby the diameter of spheres gets bigger. **Fig. 14** shows SEM images of 3.5 wt% PAN-0.05 wt% TEGO before and after carbonization. The average diameter of spheres before carbonization is about 6.5 μm. In **Fig. 14b** and **14c**, one can immediately notice an interesting microstructure composed of two disjointed spheres which might have been formed due to phase separation because of high TEGO amount in electrospun solution. EDX results confirm that the average carbon wt% in outer sphere shell is about 71 whereas the inner sphere shell has 62 % carbon. High carbon content in outer sphere and the wrinkles in **Fig. 14b** point to the high amount of graphene sheets and less polymer intercalation in the outer part of the structure. Consequently, TEGO starts phase separation after the complete diffusion of polymer chains through graphene layers and spheres are entwined together and isolated from each other. Moreover, since the inner layer should have smaller viscosity than the outer layer referring to the graphene content as measured by the EDX, during electrospraying process, the inner layer should be deformed much easier than the outer layer by the combined surface forces (i.e., electric and surface tension forces).

After heat treatment, TEGO based PAN spheres collapses totally and the boundaries on the surface of layers and the smooth surfaces are clearly seen in **Fig. 14d**. When compared to the results having high polymer concentration and low TEGO amount given in **Fig. 13**, the porosity of surfaces in **Fig. 14** decreases significantly by increasing TEGO and reducing polymer concentration. These results confirmed the significance of solvent evaporation rate, solution viscosity, polymer concentration and TEGO amount on sphere morphology.

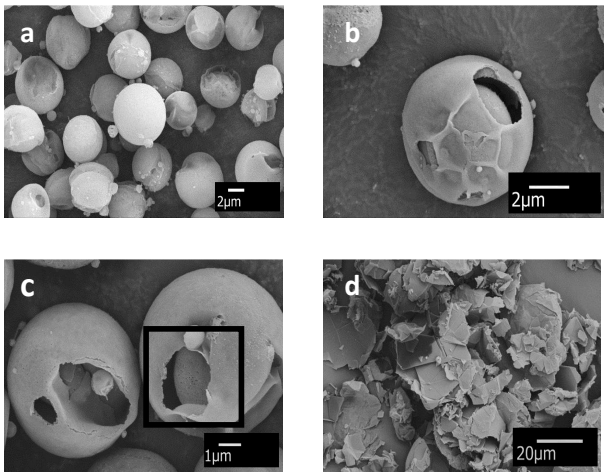

Fig. 14 SEM images of 3.5 wt% PAN-0.05 wt% TEGO spheres (a-c) before and (d) after carbonization.

Raman spectra of TEGO and 5 wt% PAN-0.02 wt% TEGO spheres before and after carbonization are shown in **Fig. 15a**. In the Raman spectrum of carbonized TEGO based PAN spheres, two peaks appears: the peak at ~1340 cm^{-1} related to D band of graphene and the peak around ~1580 cm^{-1} attributed to G band. I_D/I_G ratio of carbonized spheres is approximately 0.9 higher than I_D/I_G ratio of TEGO as 0.2 which shows the growing of graphene-like structures and reordering of aromatic groups towards graphene networks at higher temperatures[46]. **Fig. 15b** shows FTIR spectra of TEGO and produced PAN spheres. In the FTIR spectrum of TEGO, there is no sharp peak since thermal exfoliation of GO removes most of the oxygen functional groups and the resultant material has high carbon content. Only a weak peak at around 1722 cm^{-1} appears which is assigned to carbonyl stretching of C=O[47]. PAN spheres show characteristic peaks at 2930 cm^{-1}, 2250 cm^{-1}, and 1450 cm^{-1} which are associated with C-H bonds in CH_2, nitrile bond (C≡N), and tensile vibration of CH_2, respectively[48]. By the incorporation of TEGO into the structure, a sharp peak at 1720 cm^{-1} can be distinguished easily related to the stretching vibration from carbonyl group (C=O) of TEGO. Thus, this confirms the presence of TEGO in the structure. After applying heat treatment, the reduction in peak intensities at 2930 cm^{-1} and 1450 cm^{-1} and the disappearance of the peak at 2250 cm^{-1} indicate the cyclization and dehydrogenation of TEGO based PAN spheres during carbonization process.

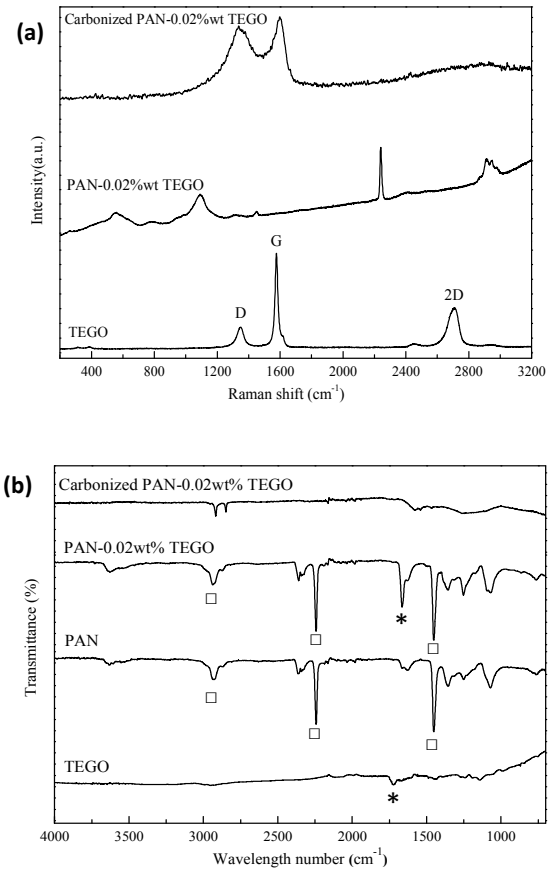

Fig. 15 (a) Raman spectra and (b) FTIR spectra of TEGO, and 5 wt % PAN-0.02 wt% TEGO spheres before and after carbonization. (□ and * signs in the FTIR spectra represent PAN and TEGO characteristic peaks, respectively).

Conclusions

In this study, hollow and filled graphene based polymeric spheres are successfully produced by using core-shell electrospraying technique. Without applying any post treatment or using any template, it is possible to control the hollowness of spheres by using core solvent and changing its flow rate in one-step process. This technique also diminishes crumbling and agglomeration of 2D graphene sheets and provides better dispersion of graphene layers through polymer chains. In this study, PS and PMMA are used as carrier polymers to convert 2D graphene sheets into 3D dimensional spheres since these polymers are easily processable for bead formation and are widely used as templates to produce hollow structures. In addition, PAN polymer is preferred as a carrier polymer to improve connections between TEGO sheets, and after carbonization, carbon content of spheres and graphene-like growing significantly increase. Decreasing PAN concentration and increasing TEGO amount lead to the formation of disjointed spheres in the same structure and this phenomenon is still under investigation. The control of solution parameters in bead formation might give new direction to several applications including aerosols, surface coatings, membranes, and drug delivery systems. In order

to find the proper concentration for the fabrication of polymeric spheres, a new diagram based on concentration and molecular weight of PMMA, PS and PAN in DMF solvent is constructed by using Mark-Houwink-Sakurada equations. The obtained data from the diagram is consistent with the experimental results. In the presence of graphene in the sphere structure, the intercalation and shifting in XRD patterns towards lower angles indicate the presence of graphene sheets in polymer matrix. In the proposed technique, the number of polymeric shells can be increased by increasing syringe number in electrospraying set-up, and multi-layer composite spheres having enhanced multi-functionality can be produced by using different polymers with different degree of hydrophilicity. In addition, catalysts can be deposited on the surface of polymeric shells and electrolytes can be inserted in core part during electrospraying. Consequently, multi-axial core shell electrospraying technique will increase accessible surface area of 2D graphene sheets and preserve characteristic properties of graphene in bulk systems, and open up new directions especially in energy applications such as Li-ion batteries, fuel cells, and supercapacitors.

Supporting Information

The Chemical structures of (a) PMMA, (b) PS, and (c) PAN polymers, table of electrospraying parameters of PS-TEGO, PMMA-TEGO, and PAN-TEGO spheres, table of positions and intensities of D, G, 2D peaks, ID/IG and IG/I2D values of untreated TEGO, sonicated and electrosprayed TEGO, table of Mark-Houwink-Sakurada constants for PMMA, PS, and PAN polymers at room temperature, table of XRD diffraction peak intensities and positions of TEGO based PMMA and PS based spheres, table of Raman peak intensities of PS and PS-0.02 wt% TEGO spheres, and SEM image of PMMA spheres containing 0.02 wt% TEGO using methanol as a core material with the flow rate of 5 µL/min. This material is available free of charge via the Internet at *www.rsc.org/advances/.*

Acknowledgements

The authors acknowledge financial support from the Scientific and Technical Research Council of Turkey (Tubitak) Project No: 112M312, COST MP1202, 2130018 and 114F029 and thank to Assoc. Prof. German Salazar Alvarez and his PhD student Valentina Guccini from Stockholm University for SEM characterization, Dr. Serap Hayat Soytas from Sabanci University for the synthesis of PAN polymer, and Dr. Meltem Sezen and her MSc student Sina Sadighikia from Sabanci University Nanotechnology Research and Application Center for FIB-SEM analysis.

References

1 T. Kuilla, S. Bhadra, D. Yao, N. H. Kim, S. Bose and J. H. Lee, *Prog. Polym. Sci.*, 2010, **35**, 1350–1375.

2 B. Luo, S. Liu and L. Zhi, *Small*, 2012, **8**, 630–646.

3 K. Coleman and R. S. Edwards, *Nanoscale*, 2012, 38–51.

4 Y. Ma and Y. Chen, *Natl. Sci. Rev.*, 2014, **2**, 40–53.

5 Z. Zhang, F. Xiao and S. Wang, *J. Mater. Chem. A*, 2015, **3**, 11215–11223.

6 Y. Zhao, C. Jiang, C. Hu, Z. Dong, J. Xue, Y. Meng, N. Zheng, P. Chen and L. Qu, *ACS Nano*, 2013, **7**, 2406–2412.

7 C. Hu, Y. Zhao, H. Cheng, Y. Wang, Z. Dong, C. Jiang, X. Zhai, L. Jiang and L. Qu, *Nano Lett.*, 2012, **12**, 5879–5884.

8 J. S. Lee, S. I. Kim, J. C. Yoon and J. H. Jang, *ACS Nano*, 2013, **7**, 6047–6055.

9 Z. Zhang, F. Xiao, L. Qian, J. Xiao, S. Wang and Y. Liu, *Adv. Energy Mater.*, 2014, **4**, 1400064.

10 B. G. Choi, M. Yang, W. H. Hong, J. W. Choi and Y. S. Huh, *ACS Nano*, 2012, **6**, 4020–4028.

11 Z. Chen, W. Ren, L. Gao, B. Liu, S. Pei and H.M. Cheng, *Nat. Mater.*, 2011, **10**, 424–428.

12 Z. Liu, Z. Tu, Y. Li, F. Yang, S. Han, W. Yang, L. Zhang, G. Wang, C. Xu and J. Gao, *Mater. Lett.*, 2014, **122**, 285–288.

13 US20120128573 A1, 2012, 1.

14 P. Guo, H. Song and X. Chen, *J. Mater. Chem.*, 2010, **20**, 4867.

15 Z. Zhang, F. Xiao, Y. Guo, S. Wang and Y. Liu, *ACS Appl. Mater. Interfaces*, 2013, **5**, 2227–2233.

16 Z. Zhang, L. Wang, J. Xiao, F. Xiao and S. Wang, *ACS Appl. Mater. Interfaces*, 2015, **7**, 17963–17968.

17 Z. Zhang, G. Chen, H. Wang and W. Zhai, *J. Mater. Chem. C*, 2015, **3**, 1649–1654.

18 K. Xu, G. Chen and D. Qiu, *J. Mater. Chem. A*, 2013, **1**, 12395.

19 K. Xu, G. Chen and D. Qiu, *Chem. Asian J.*, 2015, **10**, 1225–1231.

20 K. Chi, Z. Zhang, J. Xi, Y. Huang, F. Xiao, S. Wang and Y. Liu, *ACS Appl. Mater. Interfaces*, 2014, **6**, 16312–16319.

21 Z. Zhang, F. Xiao, J. Xiao and S. Wang, *J. Mater. Chem. A*, 2015, **3**, 11817–11823.

22 Q. Shao, J. Tang, Y. Lin, F. Zhang, J. Yuan, H. Zhang, N. Shinya and L.C. Qin, *J. Mater. Chem. A*, 2013, **1**, 15423–15428.

23 L. Wu, H. Feng, M. Liu, K. Zhang and J. Li, *Nanoscale*, 2013, **5**, 10839–43.

24 Z. Zhang, F. Xiao, J. Xi, T. Sun, S. Xiao, H. Wang, S. Wang and Y. Liu, *Sci. Rep.*, 2014, **4**, 4053.

25 Y. Xu, Y. Zhu, F. Han, C. Luo and C. Wang, *Adv. Energy Mater.*, 2014, 1–7.

26 Z. Sun, E. Zussman, A. L. Yarin, J. H. Wendorff and A. Greiner, *Adv. Mater.*, 2003, **15**, 1929–1932.

27 A. K. Moghe and B. S. Gupta, *Polym. Rev.*, 2008, **48**, 353–377.

28 N. Promphet, P. Rattanarat, R. Rangkupan, O. Chailapakul and N. Rodthongkum, *Sensors Actuators B Chem.*, 2015, **207**, 526–534.

29 C.J. Lin, C.L. Liu and W.C. Chen, *J. Mater. Chem. C*, 2015, **3**, 4290-4296.

30 S. Shilpa, B. M. Basavaraja, S. B. Majumder and A. Sharma, *J. Mater. Chem. A*, 2015, **3**, 5344–5351.

31 G. Eda and S. Shivkumar, *J. Mater. Sci.*, 2006, **41**, 5704–5708.

32 K. H. Yoon, J. Unyong and C. C. Eun, *Langmuir*, 2008, **24**, 2446–2451.

33 J. Seyyed Monfared Zanjani, B. Saner Okan, I. Letofsky-Papst, M. Yildiz and Y. Z. Menceloglu, *Eur. Polym. J.*, 2015, **62**, 66–76.

34 M. S. A. Rahaman, A. F. Ismail and A. Mustafa, *Polym. Degrad. Stab.*, 2007, **92**, 1421–1432.

35 B. Saner, F. Dinc and Y. Yürüm, *Fuel*, 2011, **90**, 2609–2616.

36 A. C. Ferrari, J. C. Meyer, V. Scardaci, C. Casiraghi, M. Lazzeri, F. Mauri, S. Piscanec, D. Jiang, K. S. Novoselov, S. Roth and A. K. Geim, *Phys. Rev. Lett.*, 2006, **97**.

37 B. Saner, F. Okyay and Y. Yürüm, *Fuel*, 2010, **89**, 1903–1910.

38 R. H. Colby, *Rheol. Acta*, 2010, **49**, 425–442.

39 D. Li, M. B. Müller, S. Gilje, R. B. Kaner and G. G. Wallace, *Nat. Nanotechnol.*, 2008, **3**, 101–105.

40 J. William, S. Hummers and R. E. Offeman, *J. Am. Chem. Soc*, 1958, **80**, 1339.

41 B. S. Okan, A. Yürüm, N. Gorgülü, S. A. Gürsel and Y. Yürüm, *Ind. Eng. Chem. Res.*, 2011, **50**, 12562–12571.

42 R. Zhang, Y. Hu, J. Xu, W. Fan and Z. Chen, *Polym. Degrad. Stab.*, 2004, **85**, 583–588.

43 T. N. Blanton and D. Majumdar, *Powder Diffr.*, 2012, **27**, 104–107.

44 A. Palm, *J. Phys. Chem.*, 1951, **55**, 1320–1324.

45 A. Arinstein and E. Zussman, *J. Polym. Sci. Part B Polym. Phys.*, 2011, **49**, 691–707.

46 J. McDonald-Wharry, M. Manley-Harris and K. Pickering, *Carbon N. Y.*, 2013, **59**, 383–405.

47 M. Naebe, J. Wang, A. Amini, H. Khayyam, N. Hameed, L. H. Li, Y. Chen and B. Fox, *Sci. Rep.*, 2014, **4**, 4375.

48 S. Lee, J. Kim, B.C. Ku, J. Kim and H.I. Joh, *Adv. Chem. Eng. Sci.*, 2012, **02**, 275–282.